ACS Biomaterials SCIENCE & ENGINEERING

pubs.acs.org/journal/abseba

Article

Effect of Matrix Stiffness on the Osteogenic Differentiation of Human Periodontal Ligament Stem Cells in a Three-Dimensional Culture Hydrogel: A Preliminary Study

Shiyang Wu,[§] Zhen Chai,[§] Yanshen Yang, Rong Ding, Bei Gao, Chen Chen, Siyu He, Zhuofu Zhang, Wanting Wan,* and Rui Zou*

Cite This: *ACS Biomater. Sci. Eng.* 2025, 11, 5616–5626

Read Online

ACCESS | Metrics & More | Article Recommendations | Supporting Information

ABSTRACT: Two-dimensional (2D) models fail to mimic a three-dimensional (3D) environment in studying mechanosensing of stem cells. Here, we present a 3D culture model to investigate how 3D matrix stiffness influences YAP activation and osteogenic differentiation of human periodontal ligament stem cells (hPDLSCs) and evaluate the osteogenic potential of hydrogels in vivo. In this study, a 3D culture model with an adjustable matrix stiffness was established. In the in vitro study, first the osteogenic differentiation of hPDLSCs by the expression of OCN, ALP, COL-1, and RUNX-2 was assessed using qRT-PCR, accompanied by ALP staining, and then YAP expression was evaluated by immunofluorescence. In the in vivo study, hPDLSCs, together with gelatin methacrylate (GelMA) hydrogels of different stiffnesses, were implanted into a rat alveolar bone defect model. As matrix stiffness increased, hPDLSCs showed reduced spreading and significantly decreased expression of OCN, ALP, COL-1, RUNX-2, and YAP activation. Specifically, COL-1 expression in the low-stiffness group was 4.3-fold higher than that in the high-stiffness group, and the YAP nuclear/cytoplasmic ratio under low stiffness was 5.5-fold greater than that under high stiffness at day 7. In vivo, the soft-matrix-cell-laden group exhibited more new bone (86.04%) and collagen formation (74.43%) in the defect area than other groups at week 6. Reduced matrix stiffness likely promotes hPDLSC proliferation, spreading, and osteogenic differentiation through YAP activation, and low-stiffness GelMA hydrogels loaded with hPDLSCs significantly enhance alveolar bone regeneration in vivo.

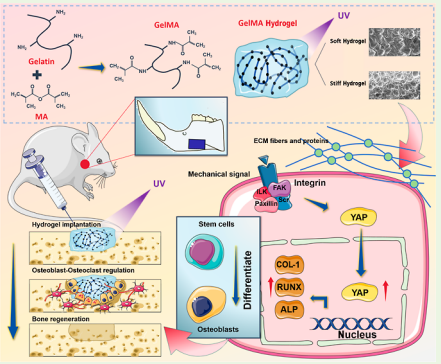

KEYWORDS: *matrix stiffness, human periodontal ligament stem cells, osteogenic differentiation, Yes-associated protein, GelMA hydrogel*

1. INTRODUCTION

Orthodontic treatment aims to reposition misaligned teeth by inducing periodontal tissues remodeling through the application of orthodontic forces.[1] Periodontal ligaments (PDLs) are biomechanically active tissues within the periodontium, essential for enduring cyclic mechanical forces and transmitting them from the teeth to the alveolar bone. These tissues exhibit mechanical adaptability and have the ability to remodel, ensuring the maintenance of their structural integrity.[2,3] Previous studies have discovered that the stiffness of PDLs changes during the othodontic tooth movement (OTM), which may be a key link in inducing periodontal tissue remodeling. Human periodontal ligament stem cells (hPDLSCs) are stem cells in the human PDLs, exhibiting characteristics and mechanical sensitivity similar to mesenchymal stem cells. They can respond to changes in the local mechanical microenvironment, such as stretching, compression, and matrix stiffness, which in turn affect their cell fate.[4,5] Detailed molecular mechanisms are being further explored.

A central molecular mechanism in this process is the regulation of the Yes-associated protein (YAP). Acting as a key effector in the integrin-cytoskeleton signaling pathway, YAP governs cellular responses to mechanical cues from the extracellular matrix (ECM). Its dynamic shuttling between the cytoplasm and nucleus is modulated by matrix stiffness and cellular tension, ultimately influencing cell behavior and gene expression.[6] Multiple studies have confirmed that YAP functions as a mechanosensory switch by detecting changes in ECM composition and mechanics, and that its nuclear localization in response to matrix stiffness plays an essential role in regulating cell behavior.[6,7] Our previous research established cell culture models with varying matrix stiffnesses and confirmed that changes in matrix stiffness can induce YAP nuclear localization, thus mediating osteogenic differentiation of cells.[8] These conclusions are mostly drawn from in vitro

Received: June 26, 2025
Revised: August 18, 2025
Accepted: August 19, 2025
Published: August 26, 2025

https://doi.org/10.1021/acsbiomaterials.5c01151
ACS Biomater. Sci. Eng. 2025, 11, 5616–5626

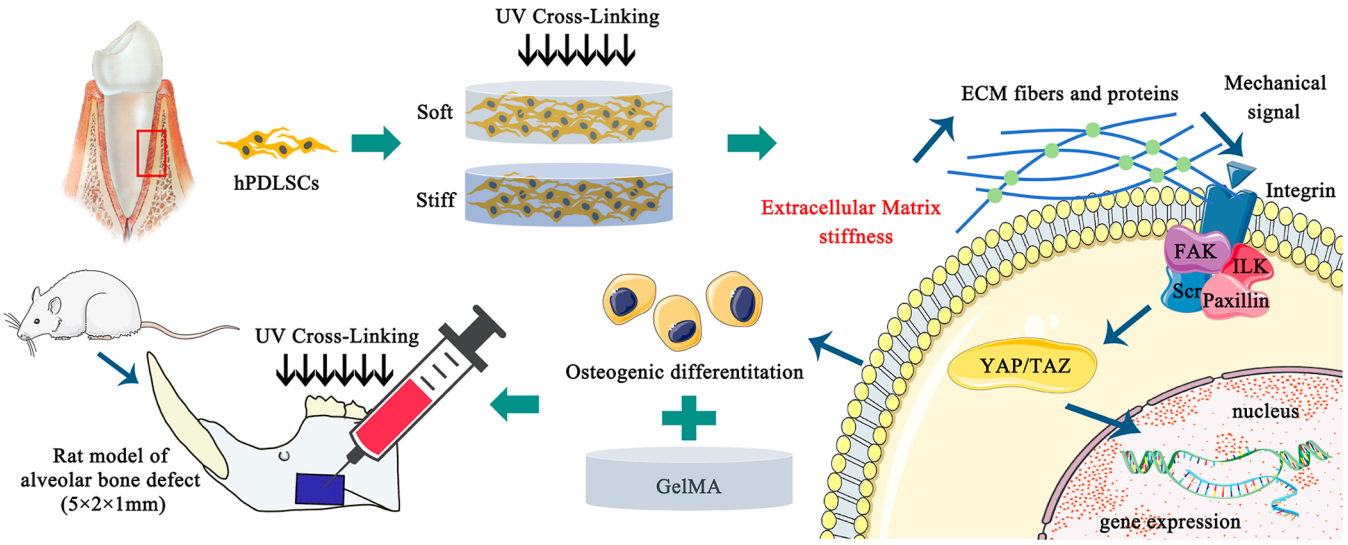

Figure 1. Schematic of this study summarizing how three-dimensional matrix stiffness affects the proliferation and osteogenic differentiation of hPDLSCs in an in vitro and in vivo model and YAP plays an essential role in this procedure. hPDLSCs were obtained using the enzyme digestion of periodontal ligaments. Graded increase stiffness of matrix was constructed by graded increase concentrations of GelMA hydrogels with ultraviolet light (UV) cross-linking. The nuclear-to-cytoplasmic ratio of YAP in hPDLSCs cultured within hydrogels of varying stiffnesses was preliminarily investigated and the ability of cell-laden hydrogels with different stiffnesses to repair alveolar bone tissue defects was evaluated in vivo.

two-dimensional (2D) cell cultures, which fail to fully replicate the in vivo conditions of the cells. In comparison to 2D cultures, the main advantage of using three dimentional (3D) cultures is their ability to generate more complex, stable, and physiologically relevant cell models.[9] These models help to improve our understanding of cellular processes and responses. Additionally, 3D cell cultures address ethical concerns associated with the use of animal models for drug testing. As a result, 3D cell culture has become a focal point in recent years for studying cellular behavior in vitro.[10,11]

Hydrogels are essential in 3D culture systems for their softness, biocompatibility, and responsiveness, enabling applications in tissue engineering and drug delivery.[12] Gelatin methacrylate (GelMA) hydrogel, with tunable stiffness and cell compatibility, excels as a scaffold for 3D culture and bioprinting.[13,14] In this study, GelMA hydrogels of varying concentrations, simulating different matrix stiffness, were utilized to construct a 3D cell culture model, aimed at investigating the influence of matrix stiffness on hPDLSCs fate and the regulatory role of YAP. Stem cells with osteogenic differentiation capacity were coinjected with the hydrogels into a rat alveolar bone defect model to evaluate the osteoinductive potential of cell-laden GelMA hydrogels. A schematic diagram of the methods for developing this study is depicted in Figure 1. This study aims to provide novel insights into exploring the molecular mechanisms of periodontal remodeling and periodontal tissue repair strategies.

2. MATERIALS AND METHODS

2.1. Preparation of the Gelatin Methacrylate Hydrogel. GelMA was synthesized by polymerizing gelatin (Beyotime, China) and methacrylic anhydride (Aladdin, US). 10 g portion of gelatin powder was slowly dissolved in 100 mL of preheated phosphate-buffered saline (PBS; Boster, China) at 55 °C under magnetic stirring (DLAB, China) for 1 h. When the solution turned uniformly pale yellow, 6 mL of methacrylic anhydride was then added dropwise at a flow rate of 6 mL/h using a microinfusion pump (Howkmed, China). The reaction mixture was stirred continuously for 4 h. 400 mL of preheated PBS was added to dilute the solution, which was then transferred to dialysis bags (molecular weight cutoff: 8000−14 000 Da; Sigma-Aldrich) for 1 week dialysis, with the water replaced every 24 h. The dialyzed solution was filtered through a 0.22 μm membrane filter (Millex) and freeze-dried after prefreezing at −80 °C to obtain GelMA foam.

Hydrogels with varying stiffnesses were prepared by dissolving GelMA foam in α-minimum essential medium (αMEM; Gibco) preheated to 55 °C at mass-to-volume ratios of 5%, 10%, and 15%. A 1% (w/v) photoinitiator solution of lithium phenyl-2,4,6-trimethylbenzoylphosphinate (LAP; Macklin, China) was added and mixed in the dark. Cross-linking was induced under 405 nm UV light for 30 s. For morphological analysis, the hydrogels were freeze-dried, gold-coated, and imaged via scanning electron microscopy (SEM; Hitachi, Japan). Mechanical properties were evaluated by using a rheometer (Anton Paar, China).

2.2. Cell Culture and Identification. Primary hPDLSCs were cultured following established protocols approved by the Ethics Committee of the College of Stomatology, Xi'an Jiaotong University (No. [2022]022). At 80% confluence, cells were passaged by digestion with trypsin (Gibco) at 37 °C for 1−2 min, neutralized with α-minimum essential medium (αMEM) containing 10% fetal bovine serum (FBS), and centrifuged at 1000 rpm for 5 min. The resuspended cells were seeded onto substrates and cultured for 24 h before medium replacement. For osteogenic induction, third-passage hPDLSCs were incubated for 21 days in an osteogenic medium containing 0.1 μg/L dexamethasone, 10 mmol/L β-glycerophosphate, and 50 μg/mL ascorbic acid (Sigma). Mineralized nodules were stained in neutral red (Solarbio). Adipogenic induction was performed using Cyagen adipogenic medium with lipid droplets stained by oil red O (Solarbio) after 14 days.

2.3. Establishment of the 3D hPDLSCs Culture Model in GelMA. GelMA solutions (5%, 10%, 15%) with 1% LAP were prepared in preheated αMEM (55 °C). hPDLSCs were resuspended in GelMA solution at 10^6 cells/mL and added dropwise to a curing ring, followed by exposure to 405 nm UV light for 30 s. After gelation, the hydrogel was placed in a well plate with complete medium and incubated, with medium changes every 2 days.

2.4. Calcein-AM/PI Staining. Cell viability of hPDLSCs in GelMA hydrogels with varying stiffnesses was assessed using Calcein-AM/PI staining (Solarbio, China). A staining solution was prepared by adding 5 μL of Calcein-AM and 15 μL of PI to 5 mL of 1× Assay Buffer. On days 1, 4, and 7, cell-laden hydrogels were washed with

https://doi.org/10.1021/acsbiomaterials.5c01151
ACS Biomater. Sci. Eng. 2025, 11, 5616−5626

Table 1. Primer Sequences for Quantitative Real-Time PCR

number	name	sequence	purpose segment
1	GAPDH-F	ACCCACTCCTCCACCTTTG	108bp
	GAPDH-R	CACCACCCTGTTGCTGTAG	
2	OCN-F	CAGGCGCTACCTGTATCAATGGC	118bp
	OCN-R	GCCGATGTGGTCAGCCAACTC	
3	RUNX2-F	CCGCCTCAGTGATTTAGGGC	132bp
	RUNX2-R	GGGTCTGTAATCTGACTCTGTCC	
4	ALP-F	ACCACCACGAGAGTGAACCA	79bp
	ALP-R	CGTTGTCTGAGTACCAGTCCC	
5	COL1-F	GCCAAGACGAAGACATCCCA	156bp
	COL1-R	GGCAGTTCTTGGTCTCGTCA	

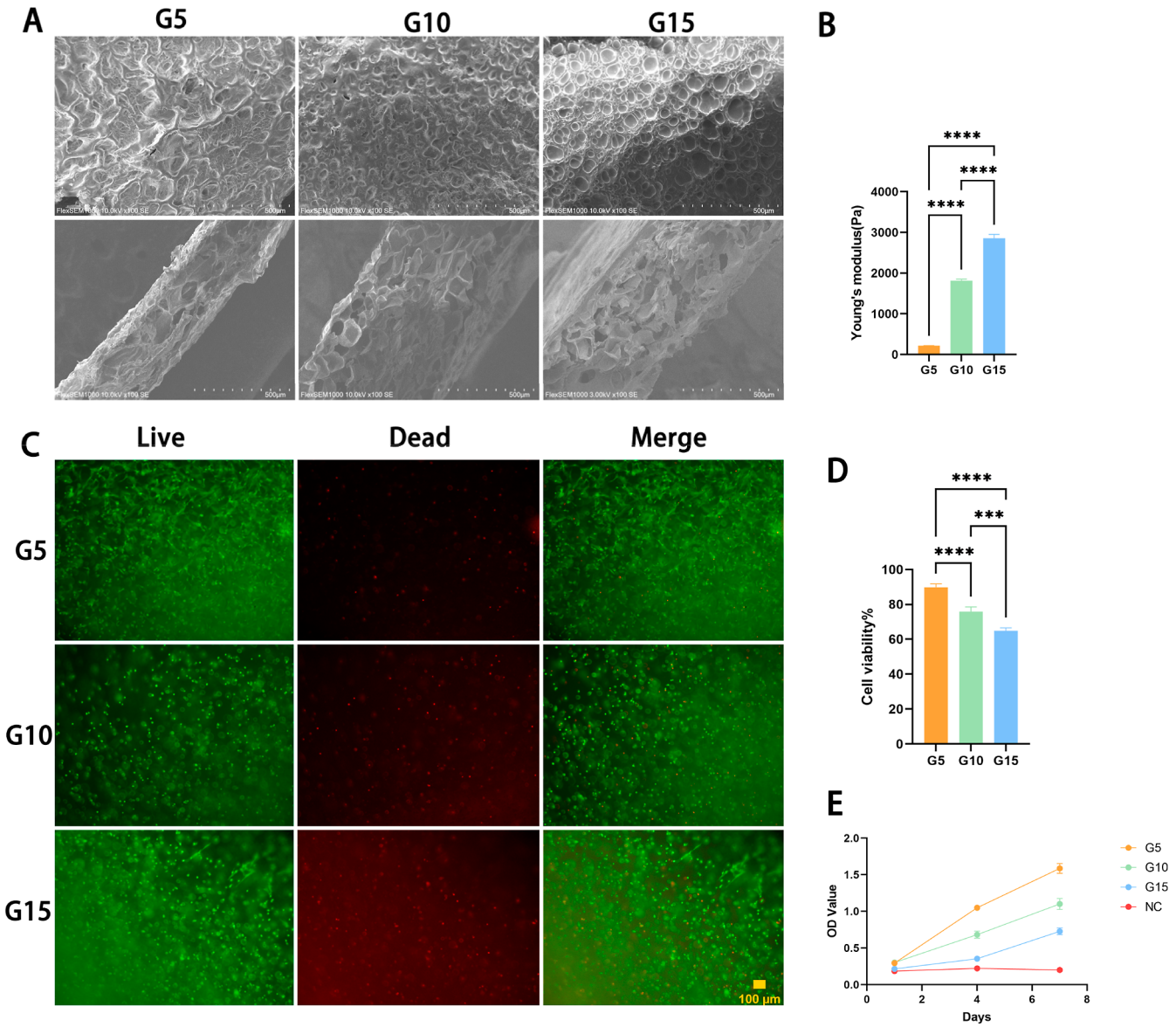

Figure 2. Characterization of the morphology and biocompatibility of GelMA hydrogels with varying stiffnesses. (A) SEM images of GelMA surfaces and sections with different stiffnesses. (B) Young's modulus of GelMA with different stiffnesses. (C) Calcein-AM/PI staining of hPDLSCs in GelMA hydrogels with varying stiffnesses on day 4. Scale bar:100 μm. (D) Cell viability analysis of hPDLSCs in GelMA hydrogels with varying stiffnesses on day 4. (E) Proliferation of hPDLSCs in hydrogels with varying stiffnesses on days 1, 4, and 7. Data are presented as means ± standard deviations (n = 3); G5, G10, and G15 represent GelMA concentrations (w/v); *p < 0.05, **p < 0.01, ***p < 0.001, ****p < 0.0001, ns: no significance.

Assay Buffer, stained for 15−30 min at 37 °C, and observed under a confocal microscope. Live cells were green and dead cells were red.

2.5. Cell Counting Kit-8 Test. Proliferation was measured using the Cell Counting Kit-8 (CCK-8, Beyotime, China). On days 1, 4,

https://doi.org/10.1021/acsbiomaterials.5c01151
ACS Biomater. Sci. Eng. 2025, 11, 5616−5626

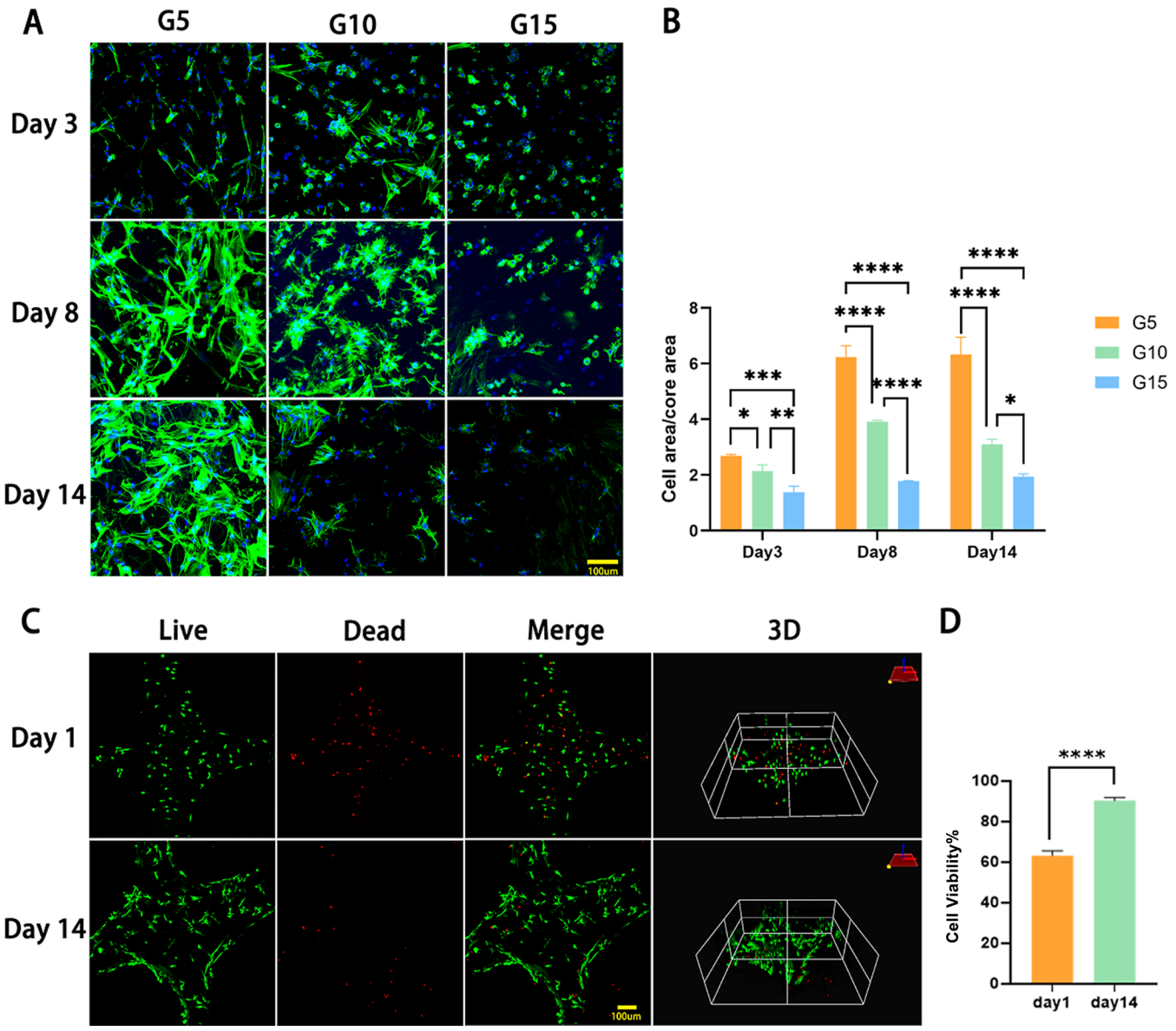

Figure 3. Spreading of hPDLSCs in GelMA hydrogels and GelMA-printed scaffolds. (A) Actin-Tracker staining of hPDLSCs cultured in GelMA hydrogels with varying stiffnesses on days 3, 8, and 14; scale bar:100 μm. (B) Cell spreading area/core area in each group. (C) Calcein-AM/PI staining of hPDLSCs in 3D-printed GelMA hydrogel scaffolds on days 1 and 14. (D) Cell viability analysis of hPDLSCs in 3D-printed GelMA hydrogels on day 1 and day 14. Data are presented as means ± standard deviations (n = 3); G5, G10, and G15 represent GelMA concentrations (w/v); *p < 0.05, **p < 0.01, ***p < 0.001, ****p < 0.0001, ns: no significance.

and 7, hydrogels were washed with PBS and incubated in CCK-8 solution at 37 °C for 3 h. The absorbance was measured at 450 nm, and the OD values were analyzed.

2.6. Cell Cytoskeleton Staining. Cell spreading on days 3, 8, and 14 was assessed using Actin-Tracker Green-488 (Beyotime, China). Hydrogels were washed, fixed in 4% paraformaldehyde, and permeabilized with PBS containing 0.1% TritonX-100. Cells were stained with Actin-Tracker Green (1:100 in PBS with 1% bovine serum albumin [BSA] and 0.1% TritonX-100) for 30−60 min, followed by DAPI staining.

2.7. Bioprinting of Cell-Laden GelMA Hydrogel. A bioink with a cell concentration of 10^6 cells/ml GelMA solution was prepared. The scaffold dimensions were 1 × 1 × 0.2 cm, with a pore size of 1 × 1 mm. The printing conditions were 5−10 °C, 25G needle, extrusion speed of 4.5 mm/s, and layer height of 0.2 mm. After printing, the scaffold was exposed to 405 nm UV light for 30 s and cultured in complete medium.

2.8. Quantitative Real-Time Polymerase Chain Reaction. GelMA lysis buffer (EFL, China) was used to lyse gel blocks and release the encapsulated cells. Total RNA was extracted from hPDLSCs using the Steady Pure Universal RNA Extraction Kit (AG). cDNA was synthesized with PrimeScript QRT Master Mix (TaKaRa, Japan) and an S1000 reverse transcription instrument (Bio-Rad). Gene expression of RUNX2, ALP, OCN, and COL-1 was detected using an Applied Biosystems PCR instrument (Thermo) and SYBR Premix Ex *Taq*II (TaKaRa, Japan). All procedures followed reagent protocols, and primer sequences are listed in Table 1.

2.9. Alkaline Phosphatase Staining. HPDLSCs were cultured in 5%, 10%, and 15% GelMA hydrogels with growth or osteogenic induction medium for 7 days. ALP staining (Biotime, China) was performed after fixation with 4% paraformaldehyde for 15 min, followed by PBS washing. The ALP staining solution was applied and incubated in the dark for 5−30 min. After washing (3 × 5 min), images were captured.

https://doi.org/10.1021/acsbiomaterials.5c01151
ACS Biomater. Sci. Eng. 2025, 11, 5616−5626

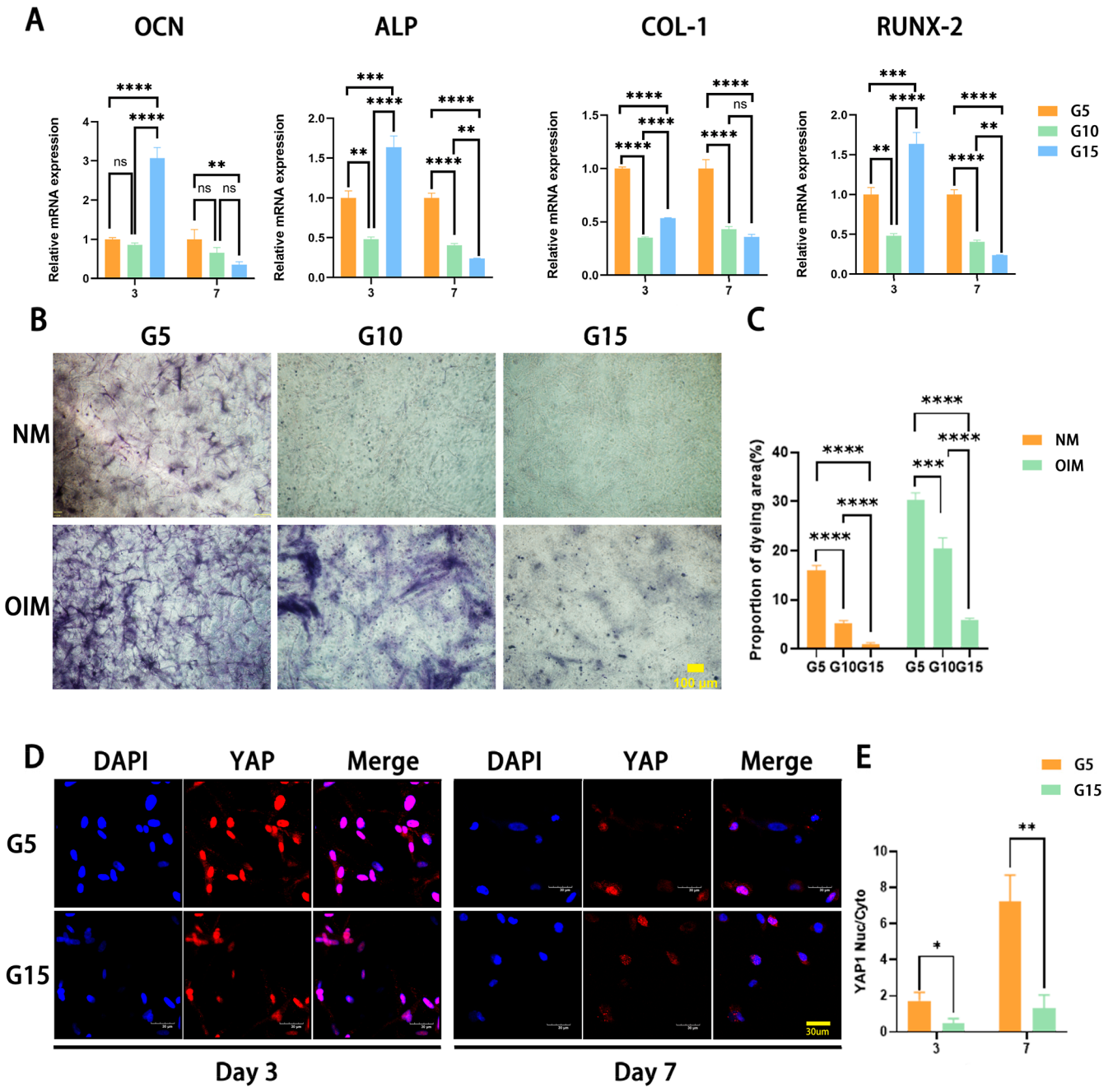

Figure 4. Effect of stiffness on the osteogenic differentiation of hPDLSCs under three-dimensional culture conditions. (A) Expression of genes associated osteogenesis with different levels of stiffness on day 3 and day 7. (B) Microscopic photographs of ALP staining of three groups at 7 days of incubation in normal medium and osteogenic induction medium. Scale bar:100 μm. (C) Statistical chart of ALP dyeing area. (D) Intracellular localization of YAP in hPDLSCs cultured in three dimensions under soft and hard stiffness on day 3 and day 7 (red fluorescence: YAP; blue fluorescence: DAPI; scale bar:30 μm). (E) Statistical chart of the nuclear-to-cytoplasmic ratio of YAP. Data are presented as means ± standard deviations (n = 3); G5, G10, and G15 represent GelMA concentrations (w/v); *p < 0.05, **p < 0.01, ***p < 0.001, ****p < 0.0001, ns: no significance.

2.10. Immunofluorescence Staining. GelMA hydrogels with hPDLSCs (soft 5% and hard 15%) were subjected to YAP protein immunofluorescence staining at days 3 and 7. Hydrogels were washed, fixed with paraformaldehyde, permeabilized with 0.2% Triton-X100, and blocked with 5% BSA. Primary anti-YAP antibody (1:100−1:200) was incubated overnight, followed by secondary antibody (1:100−1:200) for 3−4 h. DAPI staining was used for the nuclei. In each stiffness group, three biological replicates were prepared. Samples were imaged by confocal microscopy, and for each replication, three random, nonoverlapping fields were captured. YAP nuclear-to-cytoplasmic ratio (N/C ratio) was quantified using ImageJ software as YAP N/C ratio = total intensity$_{nucleus}$/total intensity$_{cytoplasm}$. Unpaired two-tailed t-tests were then performed to compare the soft and hard stiffness groups at days 3 and 7.

2.11. Constructing a Rat Alveolar Bone Defect Model. The animal experiments have been approved by the Biomedical Ethics Committee of the Xi'an Jiaotong University Health Science Center (No. 2022-1608). Thirty male SD rats (300g+) were divided into five groups (6 rats/group): blank control, 5% GelMA, 15% GelMA, 5% GelMA 3D cell-laden, and 15% GelMA 3D cell-laden. A 2 cm incision was made on the mandible, and a 5 × 2 × 1 mm defect was created. The control group received no injections, while the material groups

https://doi.org/10.1021/acsbiomaterials.5c01151
ACS Biomater. Sci. Eng. 2025, 11, 5616−5626

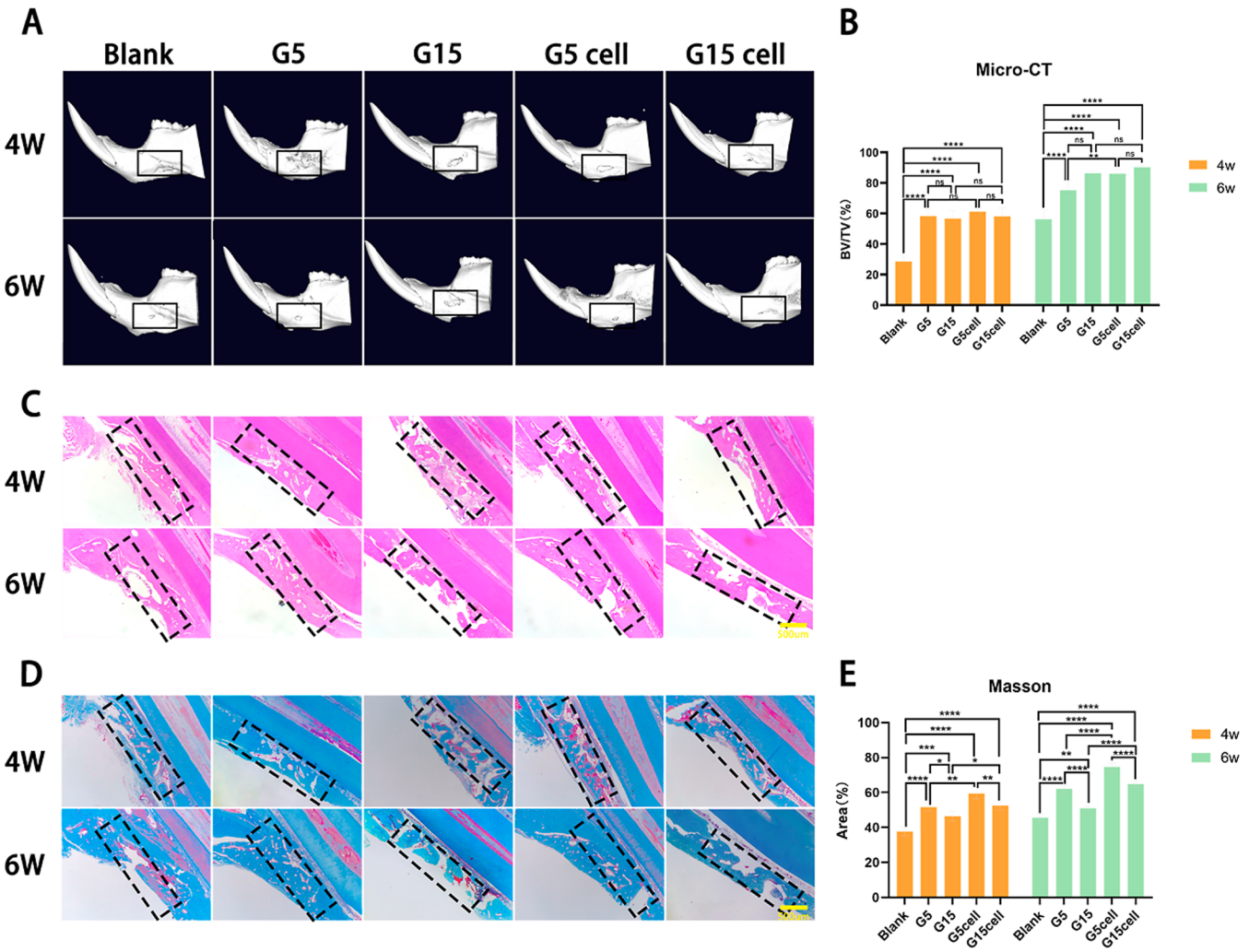

Figure 5. In vivo study of cell-laden hydrogels with varying stiffnesses for mandibular defect repair. (A) Micro-CT of each treatment group at week 4 and week 6. (B) Bone volume fraction in each treatment group at week 4 and week 6. (C) HE staining of week 4 and week 6 treated groups. The cell nucleus appears blue, and the cytoplasm appears red. Scale bar: 500 μm. (D) Masson staining of week 4 and week 6 treated groups. Collagen fibers appear blue; vascular smooth muscle fibers appear red. Scale bar: 500 μm. (E) Proportion of area of collagen in Masson staining at week 4 and week 6. Scale bar: 500 μm. Data are presented as means ± standard deviations (n = 3); G5, G10, and G15 represent GelMA concentrations (w/v); *p < 0.05, **p < 0.01, ***p < 0.001, ****p < 0.0001, ns: no significance.

received 5% or 15% GelMA hydrogel with 1% LAP. Cell-laden groups received the same hydrogel with hPDLSCs (10^6/ml). After UV curing (405 nm, 30 s), wounds were sutured, disinfected, and treated with an erythromycin ointment. Penicillin (80 000 units) was given for 3 days. Details of the surgical procedure are included in the Supporting Information (Figure S1). At weeks 4 and 6, rats were euthanized, mandibles were collected, fixed, and washed with saline, and micro-computed tomography (micro-CT) was performed (PerkinElmer, US) to calculate the progression of newly formed bone. Bone volume/tissue volume (BV/TV, %) was assessed for quantitative analysis of new bone growth within the defect area.

2.12. Hematoxylin and Eosin and Masson Staining. Hematoxylin and eosin (HE) and Masson's trichrome staining were performed to visualize tissue morphology and collagen distribution. Samples were decalcified in 10% EDTA solution, dried, and dehydrated in ethanol gradients (3 h each). They were cleared in xylene, embedded in paraffin, and sectioned to a 3 μm thickness. Sections were incubated in xylene I and II (20 min each), absolute ethanol I and II (5 min each), and 75% ethanol (5 min) and rinsed with distilled water. After staining, sections were dehydrated, cleared, and coverslipped. Images were captured using a conventional microscope (Nikon, Japan), and the newly formed collagen area was calculated as its ratio to the total defect area.

2.13. Statistical Analysis. All images were captured and quantified with ImageJ software. All statistical data were analyzed with GraphPad Prism 9.0 software and presented as the mean ± standard deviation (SD). Multiple comparisons among the three experimental groups were assessed by the ordinary one-way analysis of variance (ANOVA).

3. RESULTS AND CONCLUSION

3.1. Development of a 3D Hydrogel Culture Model with Gradient Matrix Stiffness for hPDLSCs. SEM reveals the porous structure of the GelMA hydrogel with larger pore sizes and a looser structure observed in 5% GelMA (G5). As the concentration of the hydrogel increases, the structure becomes denser, the number of pores per unit area increases, and the individual pore size decreases (Figure 2A). Moreover, as the hydrogel concentration increases, its fluidity decreases, morphological stability enhances (Figure S2), and stiffness also increases. The stiffness of 5% (G5), 10% (G10), and 15% (G15) GelMA hydrogels are 213.49 ± 6.11 Pa, 1.89 ± 0.07 kPa, and 2.94 ± 0.18 kPa, respectively, showing significant differences (p < 0.0001) (Figure 2B). The results of Calcein-

https://doi.org/10.1021/acsbiomaterials.5c01151
ACS Biomater. Sci. Eng. 2025, 11, 5616−5626

AM/PI staining showed a significantly lower number of dead cells compared to live cells, indicating robust growth of hPDLSCs within the three stiffness GelMA hydrogels after 3 days of culture (Figure 2C,D). The CCK-8 assay reveals that lower stiffness hydrogels supported greater proliferation, while increased GelMA stiffness corresponded to a significant reduction in cell proliferation rates (Figure 2E).

3.2. Spreading of hPDLSCs in GelMA Hydrogels and GelMA-Printed Scaffolds. In this study, hPDLSCs exhibit distinct spreading patterns within GelMA hydrogels of varying stiffnesses. On the eighth day of culture, bright-field images revealed that cells in low-stiffness hydrogels exhibited a larger spreading area (Figure S3). Cytoskeletal staining shows that in 5% GelMA hydrogels, cells demonstrate robust three-dimensional spreading by day 3, progressively forming a grid-like structure by day 8 and even more prominently by day 14. In contrast, 15% GelMA hydrogels show limited spreading at day 8, with overall spreading markedly reduced compared to 5% and 10% hydrogels. Notably, as GelMA stiffness increases, the cell-to-nucleus area ratio decreases significantly across the three stiffness levels ($p < 0.0001$) (Figure 3A,B).

To investigate an alternative approach for three-dimensional cell culture preparation, a 10% GelMA solution, characterized by optimal stiffness and biocompatibility, was selected as the bioink. Cell-laden GelMA hydrogels were fabricated using bioprinting, with initial postprinting cell viability observed at 63.09% on day 1, which increased to 90.30% on day 14, reflecting the contribution of cell proliferation (Figure 3C,D). At day 14, cytoskeletal staining showed that the hPDLSCs spread well within the printed scaffold (Figure S4).

3.3. Effect of Stiffness on Osteogenic Differentiation and YAP Nuclear Localization of hPDLSCs under Three-Dimensional Culture. To investigate the impact of hydrogel stiffness on the osteogenic differentiation of hPDLSCs in a three-dimensional culture, we assessed the expression levels of RUNX2, OCN, COL-1, and ALP using qRT-PCR. On day 3, the 15% GelMA group exhibited significantly higher expression levels of RUNX2, OCN, and COL-1 compared to the 5% and 10% groups (Figure 4A). However, by day 7, the expression levels of RUNX2, OCN, COL-1, and ALP decreased with increasing GelMA stiffness. ALP staining further corroborated the qRT-PCR findings, demonstrating larger, purple-stained clumps in lower-concentration GelMA hydrogels, with a significant reduction as the GelMA concentration increased. Under osteogenic induction, the areas of deep staining expanded, with 5% GelMA showing the largest stained area, followed by 10%, and the smallest in 15% GelMA (Figure 4B,C). To further investigate the nuclear localization of YAP in hPDLSCs cultured within GelMA hydrogels of varying stiffnesses, we performed YAP immunofluorescence staining on cells cultured for 3 and 7 days in both soft and stiff hydrogels. The results demonstrated that YAP was distributed in both the nucleus and cytoplasm. At day 3, cells cultured on the lower-stiffness GelMA exhibited significantly higher nuclear localization of YAP compared to those on the higher-stiffness GelMA ($p < 0.05$). By day 7, the nuclear-to-cytoplasmic ratio of YAP increased relative to day 3, indicating a trend toward YAP nuclear translocation. Furthermore, the statistical difference between the two stiffness groups at day 7 was highly significant ($p < 0.01$) (Figure 4D,E).

3.4. Repair Potential of Cell-Laden Hydrogels with Varying Stiffnesses for Rat Mandibular Defect. To evaluate the reparative potential of cell-laden hydrogels for alveolar bone defects, a rat model was established with buccal defects in the anterior teeth. The detailed grouping methodology is described in the Materials and Methods section. Bone regeneration was assessed at weeks 4 and 6 using micro-CT, HE, and Masson staining.

The results demonstrated that all material transplantation groups exhibited significantly reduced defect areas and increased bone volume fraction compared to the blank control group at both week 4 and week 6 ($p < 0.0001$). In addition, the cell-laden groups showed better regeneration than the cell-free groups; however, there was no statistically significant difference between the other groups except for the 6 week G5 group (Figure 5A,B).

The results of HE and Masson staining indicated that at weeks 4 and 6, only a small amount of new bone formation was observed in the blank control group, which was insufficient to cover the defect area. Compared with the control group, the material transplantation groups exhibited more areas of new tissue regeneration, whether loaded with hPDLSCs or not.

Masson staining results corroborated the micro-CT findings. All material-treated groups exhibited significantly greater collagen deposition compared to the blank control group ($p < 0.001$). Among them, newly formed collagen in the G15 and G15cell groups appeared relatively loose, while the soft matrix groups, particularly the G5cell group, showed denser collagen fibers, which nearly filled the entire defect area by week 6. At the same stiffness, cell-laden GelMA groups demonstrated significantly greater collagen deposition than their cell-free counterparts ($p < 0.05$). Moreover, regardless of cell loading, the low-stiffness groups exhibited higher levels of newly formed collagen than the high-stiffness groups ($p < 0.05$) (Figure 5C,D).

4. DISCUSSION

In this study, our results reveal that reduced matrix stiffness facilitates hPDLSC proliferation, spreading, and osteogenic gene expression, predominantly through the YAP pathway activation. Importantly, in vivo experiments using a rat alveolar bone defect model demonstrated that low-stiffness GelMA hydrogels loaded with hPDLSCs markedly improved bone regeneration outcomes.

Cells exist within a dynamic microenvironment that integrates not only biochemical signals but also mechanical cues.[15] The stiffness of the substrate to which cells adhere is a well-established factor that regulates key cellular processes such as migration, proliferation,[16] apoptosis, and differentiation.[17] However, most studies investigating cellular mechanosensation rely on 2D culture substrates. While this simplification enhances experimental feasibility, 2D culture fails to accurately replicate the 3D cellular microenvironment.[18] In this experiment, a 3D culture model with excellent biocompatibility and matrix stiffness gradients was established to mimic the in vivo mechanical microenvironment of the cells. The results verified the effect of matrix stiffness on the osteogenic differentiation of stem cells in a three-dimensional environment and applied this effect to promote bone repair in vitro for the first time. Recent studies have shown that stem cells adopt distinct morphologies and differentiation tendencies when cultured on substrates with a specific stiffness. For instance, mesenchymal stem cells (MSCs) cultured on soft substrates (elastic modulus: 0.1−1 kPa) tend to differentiate into neurons, while on stiffer substrates (elastic modulus: 25−40 kPa), they preferentially differentiate into osteoblasts.[17] Oh

https://doi.org/10.1021/acsbiomaterials.5c01151
ACS Biomater. Sci. Eng. 2025, 11, 5616−5626

et al. discovered that after initial adhesion, cells on the stiff substrate showed significantly better growth than those on the soft substrate.[16] In fact, it has been shown that chondrocytes are more effective at maintaining their native phenotype within a 3D matrix.[18]

GelMA hydrogels, with stiffness modulated by varying concentrations, have been extensively utilized to investigate stiffness-regulated cellular behaviors. In this study, a 3D culture model of GelMA hydrogels with gradient stiffness was successfully established. The stiffness values of 5%, 10%, and 15% GelMA hydrogels were 213.49 ± 6.11 Pa, 1.89 ± 0.07 kPa, and 2.94 ± 0.18 kPa, respectively. Although the overall matrix is relatively soft, there are statistically significant differences in the stiffness among the three hydrogel concentrations. These differences can effectively simulate the variation in substrate stiffness within soft tissues, making the hydrogels a viable platform for a 3D culture with different matrix stiffnesses.

It is noteworthy that the degradation characteristics of GelMA with varying stiffnesses were not evaluated in this study, which represents a limitation of our previous work. However, extensive research has demonstrated that higher degrees of methacrylation, increased GelMA polymer concentration, prolonged UV irradiation time, and higher photoinitiator concentrations can significantly extend the degradation time of GelMA hydrogels.[13] Shie et al. demonstrated that in a collagenase environment, 5% GelMA degraded completely within approximately 7 days, while 15% GelMA exhibited a 90% degradation rate after 14 days, which provide valuable insights and reference significance for the present work.[19]

In this study, we used a standard curing ring to prepare cell-laden GelMA hydrogels of different stiffnesses—a method that is operationally simple, quick, and cost-effective, although limited to the fixed dimensions of the curing ring. Cell viability, as assessed by CCK-8 and Calcein-AM/PI staining, demonstrated robust growth across all of the hydrogel concentrations. Furthermore, the study also explored the construction of an alternative 3D model, extrusion-based bioprinting, which demands higher equipment investment and technical proficiency but enables precise fabrication of complex geometries, stiffness gradients, and tailored cell-matrix arrangements.[20,21] We preliminarily assessed the printability of a 10% GelMA bioink laden with hPDLSCs, finding that cell viability was 63.09% on day 1 and rose to 90.30% by day 14, indicating that despite initial shear-induced cell loss, the encapsulated cells were able to survive and proliferate within the printed scaffold. These findings support the "print window" concept proposed in previous studies, confirming both the printability and biocompatibility of the material.[22,23] These results demonstrate the mechanical stability and biocompatibility of GelMA hydrogels, supporting their feasibility as bioprintable carriers for further tissue repair applications.

Generally, a stiff surface facilitates cells to spread, proliferate, and differentiate into osteoblasts under 2D matrices. Besides, these changes are always highly consistent with an increasing of the nuclear localization of YAP.[24] This discovery has been validated in various cells of human beings, such as cardiomyocytes, mesenchymal cells, and even tumor cells.[25] However, in this study, we observed that the softer matrix promotes the proliferation, spreading, and osteoblastic differentiation of hPDLSCs in a stiffness-dependent manner. The contradiction between the two dimensions (2D and 3D) has been reported in a number of studies. For example, Christine Wang discovered that polyethylene glycol (PEG) hydrogels with higher stiffness resulted in reduced tumor proliferation and spread.[26] Rizzi et al. also showed that fibroblasts can diffuse and proliferate more quickly in degradable hydrogels with a lower stiffness (241 Pa) compared to cells in hydrogels with a higher modulus (1201 Pa).[27] These results may be attributed to differences in the ECM/cell−cell interactions, trophic factors, and mechanical microenvironment between these two dimensions.[15] Cell spreading within a 3D matrix is influenced by various factors, including hydrogel density, pore size, and degradability. The stiffer matrix restricts cell spreading, which is closely linked to the proliferation. An increase in the spreading area enhances cell proliferation, whereas limited spreading results in reduced proliferation.[28,29] Another possible explanation is the deposition and remodeling of the ECM by cells. Cells perceive physical cues from the ECM, which are transduced into the cell via the focal adhesion (FA) complex on the cell membrane, allowing for ECM remodeling through complex molecular mechanisms to maintain cellular homeostasis. Studies have shown that the plasticity of 3D matrices is crucial for investigating the effects of matrix stiffness on cell behavior.[30,31] Under 3D culture, cells can sense, respond, and adapt to substrate changes more efficiently in the soft matrix, resulting in better cell spreading and proliferation activity.

The expression of osteogenesis-related genes, RUNX2, OCN, COL-1, and ALP, is an important indicator to evaluate the osteogenic differentiation and the function of bone formation.[32] They play a role in multiple stages such as osteogenic differentiation, osteocyte maturation, bone matrix mineralization, etc. The results of qRT-PCR showed that the expressions of RUNX2, OCN, COL-1, and ALP of the 15% group were significantly higher than those of the other two groups after 3 days. This may be due to the high sensitivity of cells to mechanical signals in the early stages. At this stage, the cells had not fully spread, presenting a relatively flat surface at the cellular length scale, with the local environment being more akin to a 2D setting. Thus, the local high stiffness promotes the expression of osteogenic-related genes.[33−35] However, after 7 days, the expression of these osteogenesis-related genes decreased with increasing stiffness, which was consistent with the results of the ALP staining.

We aim to explore the molecular mechanisms by which lower stiffness in 3D cell cultures promotes cell spreading and osteogenesis. Related studies have shown that ECM sense its stiffness through integrin binding, activation, and clustering, while confinement, viscoelasticity, and plasticity are detected via changes in cell volume and ion channel activation, leading to Ca^{2+} influx. ECM mechanical properties regulate the activation of proteins such as FAK, ROCK, and MLCK, involving PI3K, ERK, and Rho signaling pathways as well as transcription factors including YAP, p27, Sp1, and EGR1. However, the precise mechanisms linking ECM properties to these molecular responses remain unclear.[11]

YAP is a key downstream molecule of the focal adhesion-integrin-cytoskeleton signaling pathway and is recognized as an essential target for the study of cellular mechanosensing.[36] Acting as a transcriptional regulator, YAP metastasizes into the nucleus when it is activated. Immunofluorescence analysis showed that in the 3D culture, cell spreading was restricted in the stiff matrix, and the activated YAP ratio decreased, in contrast to the 2D culture. Notably, cell spreading, the ratio of activated YAP, and the high expression of osteogenic genes

https://doi.org/10.1021/acsbiomaterials.5c01151
ACS Biomater. Sci. Eng. 2025, 11, 5616−5626

were consistently synchronized. Cells sense mechanical changes in the ECM through the formation of the focal adhesion complex and adapt by remodeling the cytoskeleton actin.[37] Studies have confirmed that the activation of YAP/TAZ is closely related to the tension of cytoskeletal actin.[36] In 2D culture, the hard matrix increases the number of focal adhesions as well as the tension of cytoskeletal actin, which can promote YAP/TAZ activation and osteogenic differentiation by increasing the expression of osteogenic-related genes.[38] However, in 3D culture, the restriction of cell spreading may mean lower cytoskeletal tension,[39] which reduced nuclear localization of YAP and osteogenic differentiation. CTGF and CYR61 are critical downstream target genes of the YAP signaling pathway; their expression levels can serve as indicators of YAP activity. Both play major roles in fibrosis, tumorigenesis, and angiogenesis and are commonly used as biomarkers of YAP pathway activation.[40,41] Therefore, further research should be performed to investigate the relationship between the activation of YAP downstream genes and osteogenesis.

Transplantation of 3D scaffold material combined with stem cells is a vital strategy applied in tissue engineering to promote bone regeneration.[42] Hydrogel materials, with their porous biomimetic properties, can fill alveolar bone defects and facilitate repair.[43,44] This view can be well verified in this study; that is, the new bone formation and collagen deposition in the experimental group (including the cell-laden and the cell-free groups) were higher than those in the blank group. With the passage of time (week 4−week 6), the new bone formation in the blank group verified the self-healing ability of bone. Although no significant differences were observed in the micro-CT results, Masson's staining demonstrated that collagen deposition was significantly greater in the 5% hydrogel group compared to the 15% group, with the cell-laden group higher than the cell-free group. These results suggest that a soft GelMA hydrogel loaded with hPDLSCs demonstrated excellent capacity for rat alveolar bone repair. This may be due to the looser, more porous structure of the soft matrix that facilitates nutrient exchange and calcium ion flow and promotes osteogenic differentiation of stem cells.[45] There are still some limitations of this part; adding quantitative micro-CT data on bone mineral density will enhance the conclusion. Another limitation is that the coupling effect of GelMA's degradation behavior and its stiffness on osteogenesis was not explored. In future work, we plan to incorporate quantitative analysis of degradation kinetics, such as mass loss curves before and after cell encapsulation, and attempt to design controllable GelMA composite systems. By ensuring the activity and structural stability of the 3D extracellular microenvironment, we aim to systematically dissect the independent contributions of stiffness and degradability in alveolar bone regeneration.

Furthermore, numerous studies have confirmed that inflammation plays a pivotal regulatory role in tissue repair and regeneration.[46,47] Assessing the in vivo inflammatory response is instrumental for evaluating the immunocompatibility of implanted materials and guiding future immune-modulatory strategies. Future studies should quantify osteogenic markers and inflammatory cell infiltration and analyze M1/M2 macrophage ratios using immunohistochemistry and immunofluorescence techniques, dynamically tracking the transition from pro-inflammatory to anti-inflammatory phases. Deriving such multidimensional data can illuminate how the immune microenvironment regulates regeneration, thereby providing a solid foundation for immunocompatibility assessment and optimized material design.

In summary, the results demonstrated that the soft matrix enhances cell spreading, proliferation, and YAP activation, which, in turn, promotes osteogenic differentiation in a 3D environment. Additionally, we confirmed the benefits of pretreated stem cells combined with GelMA hydrogel for promoting bone regeneration in vivo. Further research into the detailed molecular mechanisms of mechanosensing within 3D matrices is crucial to advancing our understanding of periodontal tissue regeneration and guiding the development of tissue engineering.

■ ASSOCIATED CONTENT

Supporting Information

The Supporting Information is available free of charge at https://pubs.acs.org/doi/10.1021/acsbiomaterials.5c01151.

Surgical procedure for rat model establishment; gelation patterns of GelMA hydrogels at different concentrations; bright-field images of hPDLSCs cultured in GelMA hydrogels with different stiffnesses for 8 days; and images of the 3D-printed 10% cell-laden GelMA scaffold (PDF)

■ AUTHOR INFORMATION

Corresponding Authors

Wanting Wan − *Key Laboratory of Shaanxi Province for Craniofacial Precision Medicine Research, College of Stomatology, Xi'an Jiaotong University, Xi'an 710049, P. R. China*; Email: wanwantingkq@xjtu.edu.cn

Rui Zou − *Key Laboratory of Shaanxi Province for Craniofacial Precision Medicine Research, College of Stomatology, Xi'an Jiaotong University, Xi'an 710049, P. R. China*; orcid.org/0000-0003-1214-9606; Email: rainy@mail.xjtu.edu.cn

Authors

Shiyang Wu − *Key Laboratory of Shaanxi Province for Craniofacial Precision Medicine Research, College of Stomatology, Xi'an Jiaotong University, Xi'an 710049, P. R. China*

Zhen Chai − *Key Laboratory of Shaanxi Province for Craniofacial Precision Medicine Research, College of Stomatology, Xi'an Jiaotong University, Xi'an 710049, P. R. China*; orcid.org/0009-0002-6886-0034

Yanshen Yang − *Key Laboratory of Biomedical Information Engineering of Ministry of Education, School of Life Science and Technology, Xi'an Jiaotong University, Xi'an 710049, P. R. China*

Rong Ding − *Key Laboratory of Shaanxi Province for Craniofacial Precision Medicine Research, College of Stomatology, Xi'an Jiaotong University, Xi'an 710049, P. R. China*

Bei Gao − *Key Laboratory of Shaanxi Province for Craniofacial Precision Medicine Research, College of Stomatology, Xi'an Jiaotong University, Xi'an 710049, P. R. China*

Chen Chen − *Key Laboratory of Shaanxi Province for Craniofacial Precision Medicine Research, College of Stomatology, Xi'an Jiaotong University, Xi'an 710049, P. R. China*

https://doi.org/10.1021/acsbiomaterials.5c01151
ACS Biomater. Sci. Eng. 2025, 11, 5616−5626

Siyu He − *Key Laboratory of Shaanxi Province for Craniofacial Precision Medicine Research, College of Stomatology, Xi'an Jiaotong University, Xi'an 710049, P. R. China*

Zhuofu Zhang − *Key Laboratory of Shaanxi Province for Craniofacial Precision Medicine Research, College of Stomatology, Xi'an Jiaotong University, Xi'an 710049, P. R. China*

Complete contact information is available at: https://pubs.acs.org/10.1021/acsbiomaterials.5c01151

Author Contributions

[§]S.W. and Z.C. contributed equally to this work. S.W.: methodology, validation, formal analysis, writing original draft, investigation. Z.C.: methodology, validation, formal analysis, writing original draft, investigation. Y.Y.: formal analysis, methodology, visualization. R.D.: investigation, methodology, visualization. B.G.: review and editing. C.C.: review and editing. S.H.: review and editing. Z.Z.: review and editing. W.W.: review and editing, supervision, project administration. R.Z.: funding acquisition, review and editing, supervision, project administration.

Notes

Studies involving human cells: This study has been approved by the ethics committee of the College of Stomatology, Xi'an Jiaotong University (No. [2022]022). Study involving animal experiments: This study has been approved by the biomedical ethics committee of the Xi'an Jiaotong University Health Science Center (No. 2022-1608).

The authors declare no competing financial interest.

■ ACKNOWLEDGMENTS

This work was supported by the National Natural Science Foundation of China (No. 82370997).

■ REFERENCES

(1) Li, Y.; Zhan, Q.; Bao, M.; Yi, J.; Li, Y. Biomechanical and biological responses of periodontium in orthodontic tooth movement: up-date in a new decade. *Int. J. Oral Sci.* **2021**, *13* (1), 20.

(2) Lin, J. D.; Ryder, M.; Kang, M.; Ho, S. P. Biomechanical pathways of dentoalveolar fibrous joints in health and disease. *Periodontol 2000* **2020**, *82* (1), 238−256.

(3) Weider, M.; Schröder, A.; Docheva, D.; Rodrian, G.; Enderle, I.; Seidel, C. L.; Andreev, D.; Wegner, M.; Bozec, A.; Deschner, J.; et al. A human periodontal ligament fibroblast cell line as a new model to study periodontal stress. *Int. J. Oral Sci.* **2020**, *21* (21), 7961.

(4) Chaushu, S.; Klein, Y.; Mandelboim, O.; Barenholz, Y.; Fleissig, O. Immune changes induced by orthodontic forces: a critical review. *J. Dent. Res.* **2022**, *101* (1), 11−20.

(5) Li, Y.; Li, Y.; Liu, C.; Yu, X.; Gan, Z.; Xiang, L.; Zheng, J.; Meng, B.; Yu, R.; Chen, X.; et al. Mechanical force-activated CD109 on periodontal ligament stem cells governs osteogenesis and osteoclast to promote alveolar bone remodeling. *Stem Cells Transl. Med.* **2024**, *13*, 812.

(6) Dobrokhotov, O.; Samsonov, M.; Sokabe, M.; Hirata, H. Mechanoregulation and pathology of YAP/TAZ via Hippo and non-Hippo mechanisms. *Clin. Transl. Med.* **2018**, *7* (1), 23.

(7) Elosegui-Artola, A.; Andreu, I.; Beedle, A. E.; Lezamiz, A.; Uroz, M.; Kosmalska, A. J.; Oria, R.; Kechagia, J. Z.; Rico-Lastres, P.; Le Roux, A.-L.; et al. Force triggers YAP nuclear entry by regulating transport across nuclear pores. *Cell* **2017**, *171* (6), 1397.

(8) He, C.; Wang, T.; Wang, Y.; Xu, T.; Zhao, S.; Shi, H.; Zou, R. ILK regulates osteogenic differentiation of human periodontal ligament stem cells through YAP-mediated mechanical memory. *Oral Dis* **2023**, *29* (1), 274−284.

(9) Cardoso, B. D.; Castanheira, E. M.; Lanceros-Méndez, S.; Cardoso, V. F. Recent advances on cell culture platforms for in vitro drug screening and cell therapies: from conventional to microfluidic strategies. *Adv. Healthc. Mater.* **2023**, *12* (18), No. e2202936.

(10) Jensen, C.; Teng, Y. Is it time to start transitioning from 2D to 3D cell culture? *Front. Mol. Biosci.* **2020**, *7*, 33.

(11) Saraswathibhatla, A.; Indana, D.; Chaudhuri, O. Cell−extracellular matrix mechanotransduction in 3D. *Nat. Rev. Mol. Cell Biol.* **2023**, *24* (7), 495−516.

(12) Liu, X.; Liu, J.; Lin, S.; Zhao, X. Hydrogel machines. *Mater. Today* **2020**, *36*, 102−124.

(13) Yue, K.; Trujillo-de Santiago, G.; Alvarez, M. M.; Tamayol, A.; Annabi, N.; Khademhosseini, A. Synthesis, properties, and biomedical applications of gelatin methacryloyl (GelMA) hydrogels. *Biomaterials* **2015**, *73*, 254−271.

(14) Xiao, S.; Zhao, T.; Wang, J.; Wang, C.; Du, J.; Ying, L.; Lin, J.; Zhang, C.; Hu, W.; Wang, L.; et al. Gelatin methacrylate (GelMA)-based hydrogels for cell transplantation: an effective strategy for tissue engineering. *Stem Cell Rev. Rep.* **2019**, *15*, 664−679.

(15) Zhong, J.; Yang, Y.; Liao, L.; Zhang, C. Matrix stiffness-regulated cellular functions under different dimensionalities. *Biomater. Sci.* **2020**, *8* (10), 2734−2755.

(16) Oh, S. H.; An, D. B.; Kim, T. H.; Lee, J. H. Wide-range stiffness gradient PVA/HA hydrogel to investigate stem cell differentiation behavior. *Acta Biomater.* **2016**, *35*, 23−31.

(17) Engler, A. J.; Sen, S.; Sweeney, H. L.; Discher, D. E. Matrix elasticity directs stem cell lineage specification. *Cell* **2006**, *126* (4), 677−689.

(18) Callahan, L. A. S.; Ganios, A. M.; Childers, E. P.; Weiner, S. D.; Becker, M. L. Primary human chondrocyte extracellular matrix formation and phenotype maintenance using RGD-derivatized PEGDM hydrogels possessing a continuous Young's modulus gradient. *Acta Biomater.* **2013**, *9* (4), 6095−6104.

(19) Shie, M.-Y.; Lee, J.-J.; Ho, C.-C.; Yen, S.-Y.; Ng, H. Y.; Chen, Y.-W. Effects of gelatin methacrylate bio-ink concentration on mechano-physical properties and human dermal fibroblast behavior. *Polymers* **2020**, *12* (9), 1930.

(20) Daly, A. C.; Prendergast, M. E.; Hughes, A. J.; Burdick, J. A. Bioprinting for the biologist. *Cell* **2021**, *184* (1), 18−32.

(21) Xie, M.; Shi, Y.; Zhang, C.; Ge, M.; Zhang, J.; Chen, Z.; Fu, J.; Xie, Z.; He, Y. In situ 3D bioprinting with bioconcrete bioink. *Nat. Commun.* **2022**, *13* (1), 3597.

(22) Ouyang, L. Pushing the rheological and mechanical boundaries of extrusion-based 3D bioprinting. *Trends Biotechnol.* **2022**, *40* (7), 891−902.

(23) Bertassoni, L. E.; Cardoso, J. C.; Manoharan, V.; Cristino, A. L.; Bhise, N. S.; Araujo, W. A.; Zorlutuna, P.; Vrana, N. E.; Ghaemmaghami, A. M.; Dokmeci, M. R.; et al. Direct-write bioprinting of cell-laden methacrylated gelatin hydrogels. *Biofabrication* **2014**, *6* (2), 024105.

(24) Wang, X.; Ji, L.; Wang, J.; Liu, C. Matrix stiffness regulates osteoclast fate through integrin-dependent mechanotransduction. *Bioact. Mater.* **2023**, *27*, 138−153.

(25) Ebrahimighaei, R.; Sala-Newby, G. B.; Hudson, C.; Kimura, T. E.; Hathway, T.; Hawkins, J.; McNeill, M. C.; Richardson, R.; Newby, A. C.; Bond, M. Combined role for YAP-TEAD and YAP-RUNX2 signalling in substrate-stiffness regulation of cardiac fibroblast proliferation. *Biochim. Biophys. Acta Mol. Cell Res.* **2022**, *1869* (11), 119329.

(26) Wang, C.; Sinha, S.; Jiang, X.; Murphy, L.; Fitch, S.; Wilson, C.; Grant, G.; Yang, F. Matrix stiffness modulates patient-derived glioblastoma cell fates in three-dimensional hydrogels. *Tissue Eng. Part A* **2021**, *27* (5−6), 390−401.

(27) Bott, K.; Upton, Z.; Schrobback, K.; Ehrbar, M.; Hubbell, J. A.; Lutolf, M. P.; Rizzi, S. C. The effect of matrix characteristics on fibroblast proliferation in 3D gels. *Biomaterials* **2010**, *31* (32), 8454−8464.

(28) Folkman, J.; Moscona, A. Role of cell shape in growth control. *Nature* **1978**, *273* (5661), 345−349.

(29) Califano, J. P.; Reinhart-King, C. A. Substrate stiffness and cell area predict cellular traction stresses in single cells and cells in contact. *Cell. Mol. Bioeng.* **2010**, *3*, 68−75.
(30) Chatterjee, K.; Lin-Gibson, S.; Wallace, W. E.; Parekh, S. H.; Lee, Y. J.; Cicerone, M. T.; Young, M. F.; Simon Jr, C. G. The effect of 3D hydrogel scaffold modulus on osteoblast differentiation and mineralization revealed by combinatorial screening. *Biomaterials* **2010**, *31* (19), 5051−5062.
(31) Yang, X.; Sarvestani, S. K.; Moeinzadeh, S.; He, X.; Jabbari, E. Three-dimensional-engineered matrix to study cancer stem cells and tumorsphere formation: effect of matrix modulus. *Tissue Eng. Part A* **2013**, *19* (5−6), 669−684.
(32) Huang, J.; Chen, L. IL-1β inhibits osteogenesis of human bone marrow-derived mesenchymal stem cells by activating FoxD3/microRNA-496 to repress wnt signaling. *genesis* **2017**, *55* (7), No. e23040.
(33) Rammensee, S.; Kang, M. S.; Georgiou, K.; Kumar, S.; Schaffer, D. V. Dynamics of mechanosensitive neural stem cell differentiation. *Stem cells* **2017**, *35* (2), 497−506.
(34) Goetzke, R.; Keijdener, H.; Franzen, J.; Ostrowska, A.; Nüchtern, S.; Mela, P.; Wagner, W. Differentiation of induced pluripotent stem cells towards mesenchymal stromal cells is hampered by culture in 3D hydrogels. *Sci. Rep.* **2019**, *9* (1), 15578.
(35) Hogrebe, N. J.; Gooch, K. J. Direct influence of culture dimensionality on human mesenchymal stem cell differentiation at various matrix stiffnesses using a fibrous self-assembling peptide hydrogel. *J. Biomed Mater. Res. A* **2016**, *104* (9), 2356−2368.
(36) Holland, E. N.; Fernández-Yagüe, M. A.; Zhou, D. W.; O'Neill, E. B.; Woodfolk, A. U.; Mora-Boza, A.; Fu, J.; Schlaepfer, D. D.; García, A. J. FAK, vinculin, and talin control mechanosensitive YAP nuclear localization. *Biomaterials* **2024**, *308*, 122542.
(37) Kechagia, J. Z.; Ivaska, J.; Roca-Cusachs, P. Integrins as biomechanical sensors of the microenvironment. *Nat. Rev. Mol. Cell Biol.* **2019**, *20* (8), 457−473.
(38) Dupont, S.; Morsut, L.; Aragona, M.; Enzo, E.; Giulitti, S.; Cordenonsi, M.; Zanconato, F.; Le Digabel, J.; Forcato, M.; Bicciato, S.; et al. Role of YAP/TAZ in mechanotransduction. *Nature* **2011**, *474* (7350), 179−183.
(39) Chen, L.; Wu, C.; Wei, D.; Chen, S.; Xiao, Z.; Zhu, H.; Luo, H.; Sun, J.; Fan, H. Biomimetic mineralized microenvironment stiffness regulated BMSCs osteogenic differentiation through cytoskeleton mediated mechanical signaling transduction. *Mater. Sci. Eng. C* **2021**, *119*, 111613.
(40) Kuo, C.-Y.; Chang, Y.-C.; Chien, M.-N.; Jhuang, J.-Y.; Hsu, Y.-C.; Huang, S.-Y.; Cheng, S.-P. SREBP1 promotes invasive phenotypes by upregulating CYR61/CTGF via the Hippo-YAP pathway. *Endocr. Relat. Cancer* **2022**, *29* (2), 47−58.
(41) Lang, A.; Eastburn, E. A.; Younesi, M.; Nijsure, M. P.; Siciliano, C.; Pranatharthi Haran, A.; Panebianco, C. J.; Seidl, E.; Tang, R.; Alsberg, E.; et al. CYR61 delivery promotes angiogenesis during bone fracture repair. *NPJ. Regen. Med.* **2025**, *10* (1), 20.
(42) Zhou, B.; Jiang, X.; Zhou, X.; Tan, W.; Luo, H.; Lei, S.; Yang, Y. GelMA-based bioactive hydrogel scaffolds with multiple bone defect repair functions: therapeutic strategies and recent advances. *Biomater. Res.* **2023**, *27* (1), 86.
(43) Zuo, W.; Yu, L.; Zhang, H.; Fei, Q. Mineralized collagen scaffold bone graft accelerate the osteogenic process of HASCs in proper concentration. *Regen. Ther.* **2021**, *18*, 161−167.
(44) Zhan, Z.; Li, R.; Wu, Y.; Shen, X.; Fu, D.; Han, H.; Jing, P.; Li, B.; Han, F.; Meng, B. Biomimetic periosteum-bone scaffolds with codelivery of BMP-2 and PDGF-BB for skull repair. *Bone* **2025**, *190*, 117315.
(45) Wang, W.; Yeung, K. W. Bone grafts and biomaterials substitutes for bone defect repair: A review. *Bioact. Mater.* **2017**, *2* (4), 224−247.
(46) Shi, Y.; Cao, J.; Wang, Y. Rethinking regeneration: empowerment of stem cells by inflammation. *Cell Death Differ.* **2015**, *22* (12), 1891−1892.
(47) Karin, M.; Clevers, H. Reparative inflammation takes charge of tissue regeneration. *Nature* **2016**, *529* (7586), 307−315.

https://doi.org/10.1021/acsbiomaterials.5c01151
ACS Biomater. Sci. Eng. 2025, 11, 5616−5626